Analysis of Flux Limiter Sensitivity and Shock Capturing Accuracy for LES of Turbulent High-Speed Flows

Meghna Dutta* and Joseph C. Oefelein†
Georgia Institute of Technology, Atlanta, Georgia 30332-0150

It is well known that higher-order numerical schemes must be reduced to a monotonic scheme in the vicinity of shocks to eliminate spurious oscillations across them. This increases the dissipative characteristics of the scheme in a way that eliminates these errors. However, the increased dissipation is not desirable in regions away from shocks since it can severely damp important flow characteristics. The typical way in which this tradeoff is managed is through the use of flux limiters (or equivalently shock sensors), that are optimized to activate the monotonic behavior in the vicinity of a shock, but retain the high-order characteristics of the scheme elsewhere. This "optimization" problem becomes challenging in highly unsteady turbulent flow environments since the flux limiters are constructed using various gradient ratios in the flow to sense the presence of a shock. Thus, the shock capturing accuracy of flux limiters can behave poorly when used for Large Eddy Simulation (LES) of turbulent supersonic and hypersonic flows. The gradients associated with the broadband turbulence being resolved tends to activate the sensors, thus making them very "noisy" throughout the flow field instead of being activated only in the vicinity of shocks. This noisy behavior can significantly degrade the quality of the LES since it introduces significant dissipative errors that damp out important unsteady turbulent flow structures. In this work, several flux limiting and shock capturing schemes are compared for a Mach 2.5 boundary layer flow. In particular, a modified Van Leer flux limiting method's parameters are varied and evaluated. Numerical efficiency is also investigated for cost-error tradeoff assessment.

I. Introduction

In higher fidelity CFD solvers, such as Large Eddy Simulation (LES) and Direct Numerical Simulation (DNS), a large range of length scales must be resolved. To computationally simplify this problem, non-dissipative compact schemes are introduced to numerically smoothen the field, saving computational time and resources while maintaining a high degree of accuracy. However, when these schemes interact with steep gradients, they produce unfavorable oscillations[1]. In high speed flow, this occurs at shock waves. Further challenges are introduced when the flow becomes turbulent. Turbulence gradients may converge, however, due to their small scale, there is large potential for aliasing [2], which can lead to numerical instability or artificial decay of the turbulence. Gibbs phenomenon as described by Ducros[3] shows that these oscillations do not decrease in amplitude, even with a finer more resolved grid. Alternatively, non oscillating schemes also exist, but lack the same level of accuracy. For this reason, it is beneficial to create a different function, known as a flux limiter, that can identify the location of these harsh gradients and introduce artificial dissipation in order to reduce these oscillations. Optimizing flux limiters thus becomes a crucial task, as an overactive limiter would degrade the performance of the higher order compacting scheme, as the entire flow field would have this dissipation introduced. On the other hand, an under-active limiter would prevent shock detection which would lead to the aforementioned spurious oscillations and numerical instabilities.

In this study, a modified version of the van Leer flux limiting scheme is tested and compared to a baseline. In the modified van Leer limiter, a sensitivity parameter is introduced and varied and its effect on the flowfield and resultant statistics are compared. This data is then compared with DNS to benchmark and select the best sensitivity.

II. Approach

The modified van Leer flux limiting scheme is analyzed through wall-resolved large eddy simulations (WRLES) of a Mach 2.5 boundary layer flow. Scheme parameters are also varied to examine their effects on instantaneous flowfields,

*Undergraduate Research Assistant, Daniel Guggenheim School of Aerospace Engineering, 270 Ferst Drive NW
†Professor & Faculty Advisor, Daniel Guggenheim School of Aerospace Engineering, 270 Ferst Drive NW, AIAA Associate Fellow.

as well as several statistical quantities. Cases are simulated using the hybrid LES/DNS code RAPTOR. The baseline scheme is a high-order artificial dissipation scheme, which is used to establish a baseline performance metric against which the modified van Leer limiting scheme is compared. Details of the governing system of equations, limiting schemes, and case setup and design are presented below.

A. Governing equations

The LES is governed by the filtered Navier-Stokes equations, cast into non-dimensional, finite-volume form. In the following equations, overbars indicate filtered variables, where as Favre-decomposed resolved-scale variables are represented by tildes. Subfilter-scale quantities are identified by a double prime. Cartesian tensor notation with Einstein summation convention is also employed.

- Filtered Conservation of Mass:

$$\frac{\partial \overline{\rho}}{\partial t} + \frac{\partial}{\partial x_i}\left(\overline{\rho}\tilde{u}_i\right) = 0. \tag{1}$$

- Filtered Conservation of Momentum:

$$\frac{\partial}{\partial t}\left(\overline{\rho}\tilde{u}_i\right) + \frac{\partial}{\partial x_j}\left(\overline{\rho}\tilde{u}_i\tilde{u}_j + \frac{\overline{p}}{\mathrm{M}^2}\delta_{ij}\right) = \frac{\partial}{\partial x_j}\overline{\sigma}_{ij} - \frac{\partial}{\partial x_j}T_{ij}, \tag{2}$$

where, $\overline{\sigma}_{ij}$ represents the filtered viscous stress tensor,

$$\overline{\sigma}_{ij} = \overline{\frac{\mu}{\mathrm{Re}}\left[-\frac{2}{3}\frac{\partial u_k}{\partial x_k}\delta_{ij} + \left(\frac{\partial u_i}{\partial x_j} + \frac{\partial u_j}{\partial x_i}\right)\right]},$$

and T_{ij} represents the turbulent momentum flux tensor,

$$T_{ij} = \overline{\rho}\left(\widetilde{\tilde{u}_i\tilde{u}_j} - \tilde{u}_i\tilde{u}_j\right) + \overline{\rho}\left(\widetilde{\tilde{u}_i u_j''} + \widetilde{u_i''\tilde{u}_j}\right) + \overline{\rho}\widetilde{u_i''u_j''}.$$

- Filtered Conservation of Total Energy:

$$\begin{aligned}\frac{\partial}{\partial t}\left(\overline{\rho}\tilde{e}^t\right) + \frac{\partial}{\partial x_j}\left[\left(\overline{\rho}\tilde{e}^t + \overline{p}\right)\tilde{u}_j\right] = &\frac{\partial}{\partial x_j}\left[\overline{q}_j^e + \mathrm{M}^2\left(\overline{\sigma}_{ij}\tilde{u}_i\right)\right] \\ &- \frac{\partial}{\partial x_j}\left[Q_j + \mathrm{M}^2\left(T_{ij}\tilde{u}_i\right)\right] \\ &- \frac{\partial}{\partial x_j}\left[\frac{\mathrm{M}^2}{2}T_{kk}\overline{u_j''}\right] \\ &+ \frac{\partial}{\partial x_j}\left[\mathrm{M}^2\left(\overline{\sigma_{ij}u_i''}\right)\right],\end{aligned} \tag{3}$$

where the Favre-resolved total energy, internal energy, and enthalpy are represented, respectively, as

$$\begin{aligned}\tilde{e}^t &= \tilde{e} + \frac{\mathrm{M}^2}{2}\tilde{u}_i\tilde{u}_i + \frac{M^2}{2}\frac{T_{ii}}{\overline{\rho}}, \\ \tilde{e} &= \tilde{h} - \frac{\overline{p}}{\overline{\rho}}, \text{ and} \\ \tilde{h} &= \int_{\overline{p}^\circ}^{\overline{p}}\int_{\tilde{T}^\circ}^{\tilde{T}} c_p(T,p)\mathrm{d}T\mathrm{d}p.\end{aligned}$$

Energy diffusion due to heat conduction is captured in an analogous manner to the instantaneous system using Fourier's law,

$$\overline{q}_j^e = \overline{\frac{\mu}{\mathrm{Pr}}\frac{c_p}{\mathrm{Re}}\frac{\partial T}{\partial x_j}}.$$

Finally, the turbulent enthalpy flux in the filtered energy equation is

$$Q_j = \overline{\rho}\left(\widetilde{\tilde{h}\tilde{u}_j} - \tilde{h}\tilde{u}_j\right) + \overline{\rho}\left(\widetilde{\tilde{h}u_j''} + \widetilde{h''\tilde{u}_j}\right) + \overline{\rho}\widetilde{h''u_j''}.$$

The subfilter stresses and fluxes are modeled using a compressible generalization of the Smagorinsky model [4] with the scale-similarity model proposed by Speziale [5]. Geurts [6] and Stolz and Adams [7] have shown that this approach can be generalized within the mathematical formalism of inverse methods and the approximate deconvolution model. Following Erlebacher et al. [8], the deviatoric part of the turbulent momentum flux tensor appearing in Eq. (2) is given by

$$T_{ij}^{D} = -2\frac{\mu_t}{\mathrm{Re}}\left(\tilde{S}_{ij} - \frac{1}{3}\tilde{S}_{kk}\delta_{ij}\right), \tag{4}$$

where the resolved strain rate tensor, $\tilde{S}_{ij}$, is given as

$$\tilde{S}_{ij} = \frac{1}{2}\left(\frac{\partial \tilde{u}_i}{\partial x_j} + \frac{\partial \tilde{u}_j}{\partial x_i}\right). \tag{5}$$

The quantity Re is a reference Reynolds number and is an artifact of the non-dimensionalization. The Kronecker delta tensor is denoted as δ_{ij}, and the turbulent viscosity is calculated as

$$\frac{\mu_t}{\mathrm{Re}} = \overline{\rho} C_R \Delta^2 \left(\tilde{S}_{ij}\tilde{S}_{ij}\right)^{\frac{1}{2}}. \tag{6}$$

In Eq. (6), C_R is a dynamically evaluated modified Smagorinsky coefficient [9–11] and Δ is the filter width taken to be the cube-root of a given cell volume in this work. The isotropic part of the turbulent momentum flux tensor is closed using the Yoshizawa model [12] as

$$T_{ij}^{I} = \frac{2}{3} C_I \overline{\rho} \Delta^2 \tilde{S}_{kl}\tilde{S}_{kl}\delta_{ij}, \tag{7}$$

where all terms maintain their previous definitions and C_I is the isotropic Smagorinsky coefficient, also computed dynamically. The final model form is obtained by summing the isotropic and deviatoric parts.

The subfilter energy flux is modeled using the dynamic gradient diffusion model [13], which makes use of a turbulent analog of Fourier's law of heat conduction. The non-dimensional form of the model is

$$Q_j = -\frac{\mu_t}{Re}\frac{C_p}{Pr_t}\frac{\partial \tilde{T}}{\partial x_j}. \tag{8}$$

The quantity μ_t/Re takes its definition from Eq. (6) and Pr_t is a turbulent Prandtl number that is modeled dynamically.

The system of equations above are solved in parallel using the RAPTOR code framework, which has been developed with significant effort invested on verification validation, and optimization. Time integration is performed using a semi-implicity Runge-Kutta formulation, set up to be fourth-order accurate in time. The spatial scheme is second-order accurate and designed using non-dissipative, discretely-conservative, Kinetic-Energy-Preserving – Entropy-Preserving (KEP-EP) finite-volume differencing [14–18], which minimizes numerical contamination due to artificial dissipation and the artificial build up of energy at the high wavenumbers. Details on the computational approach and parallelization strategy are given by Oefelein et al. [19–21].

B. Tested Limiting Schemes

In the baseline case, no limiting scheme is applied. In the presence of strong shocks, this case would fail due to high oscillations during computation. The Van Leer limiter is defined by equation 9[22]. The modified version of the limiter in RAPTOR allow for a sensitivity input, ε, which allows for more granular control over what is detected.

$$\phi^{vl}(r) = \frac{r + |r|}{1 + r} \tag{9}$$

C. Case Setup

Cases simulate a Mach 2.5 compressible boundary layer, with the Mach 2.5 DNS case by Zhang et al [23] used as a reference DNS case. This flow was selected, as it is slow enough to converge without a limiter, but fast enough that a limiter can be applied and compared. The computational domain is smaller than the original Zhang et al [23] DNS due to computational feasibility limits. See Fig. 1 for the case schematic, including boundary conditions. Cases employ a $660 \times 255 \times 100 (nx \times ny \times nz)$ grid, with grid generation following the traditional WRLES grid stretching guidelines.

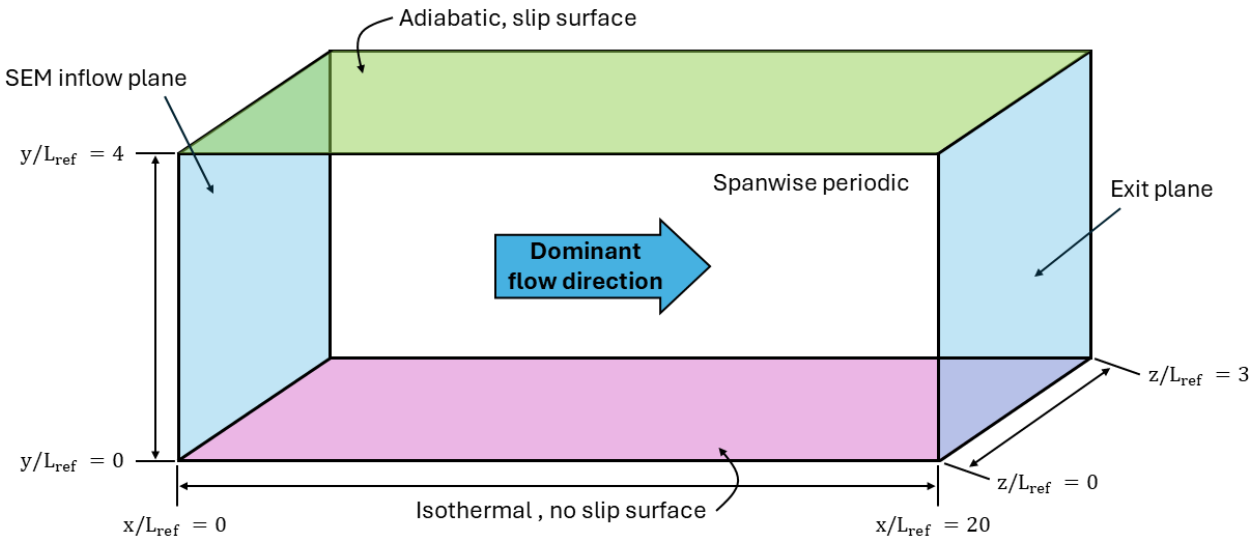

Fig. 1 Case schematic. Domain is reduced compared to the domain of the Zhang et al reference DNS case [23], due to computational feasibility reasons.

Case	Tw/Tr	Reference Data	Limiting scheme
Baseline	1.0	Zhang et al Mach 2.5 BL	N/A
mvL001	1.0	Zhang et al Mach 2.5 BL	modified van Leer
mvL01	1.0	Zhang et al Mach 2.5 BL	modified van Leer
mvL025	1.0	Zhang et al Mach 2.5 BL	modified van Leer
mvL050	1.0	Zhang et al Mach 2.5 BL	modified van Leer

Table 1 Table of case parameters. Reference data for all cases is Zhang et al [23] Mach 2.5 turbulent boundary layer DNS.

The first cell is within one y^+ unit through the domain, and cells are stretched gently away from the wall to a maximum value of $\Delta x_i^+ = 20$ for all cells, making freestream cells approximately orthogonal. While the top surface of the domain allows for waves to reflect back onto the boundary layer, the height of the domain is tall enough, and the axial length short enough, to avoid any contamination issues stemming from this confinement. Additionally, the domain is wide enough in the spanwise direction to allow for statistical decoupling, enabling the use of the spanwise periodic boundary condition.

See Table 1 for a summary of the cases including notation used in the rest of this work to refer to the cases. Inflow turbulence is generated using the ensemble synthetic eddy method [24], using the Zhang et al [23] DNS as reference data for all cases. The first case is used to establish a performance baseline and does not employ a shock-capturing scheme. The subsequent cases then systematically vary the modified van Leer parameters.

III. Results and Discussion

A. Validation

First, the baseline case is evaluated. Reynolds stresses are plotted against the reference DNS data. See Fig. 2 for the Reynolds stress results. Clearly, the results follow the overall trends quite closely, with some over-estimation.

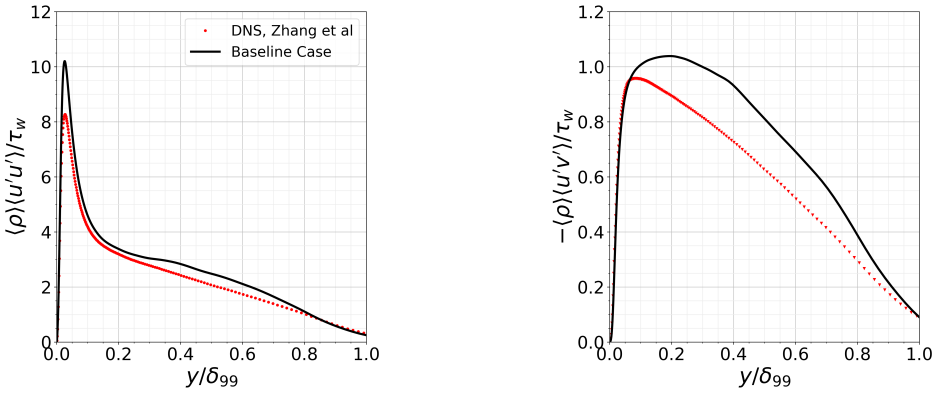

(a) R_{uu}, Streamwise Componen

(b) R_{uv}, Shear Component

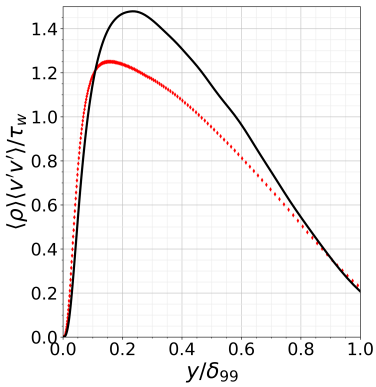

(c) R_{vv}, Wall-normal Component

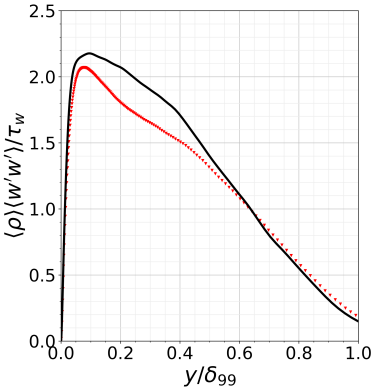

(d) R_{ww}, Spanwise Component

Fig. 2 Reynolds stresses for the baseline case compared against the reference DNS. Red symbols correspond to the reference DNS case of Zhang et al. [23]. Black solid line corresponds to the baseline case.

Additionally, see Fig. 3 for the mean velocity profile, taken at approximately $x/L_{ref} = 15.0$. Results follow the incompressible theory quite closely, with a clear linear log region. The thin black line is the incompressible log-law, given as:

$$U+ = \frac{1}{\kappa} log(y+) + B, \tag{10}$$

where κ is taken to be 0.41 and B is taken to be 5.1, is included as the thin black line. The quantity $Y+$ refers to the semi-local wall-normal coordinate. The quantity $U+_{TL}$ is the semi-local U^+. Both quantities are defined in Trettel and Larsson [25], this scaling has been found to better account for non-adiabatic walls.

B. Modified Van Leer Fields

Instantaneous and averaged plots were gathered and compared for each epsilon value tested. Every test was conducted at the same time step, so the fields were essentially the same for each limiting case. The shock is visible in Fig.4, and serves as a comparison point with each following figure. See Fig.5 and Fig.6 for the non linear and linear flux limiting scheme for each epsilon parameter. The non-linear parameter is associated with pressure, while the linear is associated with temperature and density.

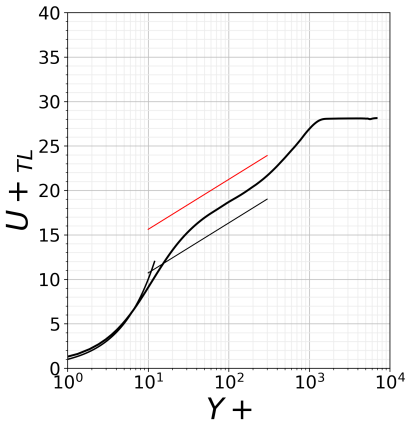

Fig. 3 Baseline case mean velocity profile compared against incompressible theory. Thin black line is the log-law given by Eqn. 10, with the thin red line corresponding to the same equation, except with y-intercept instead change to 10.

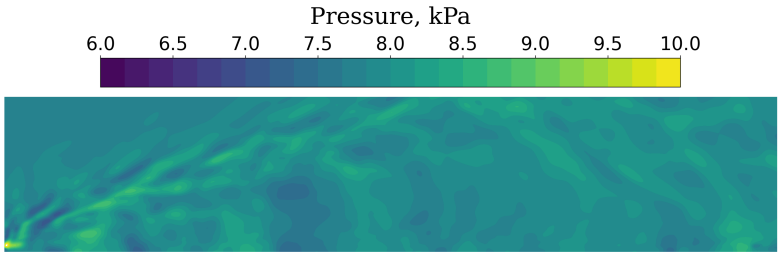

Fig. 4 Pressure distribution at the tested timestamp and conditions.

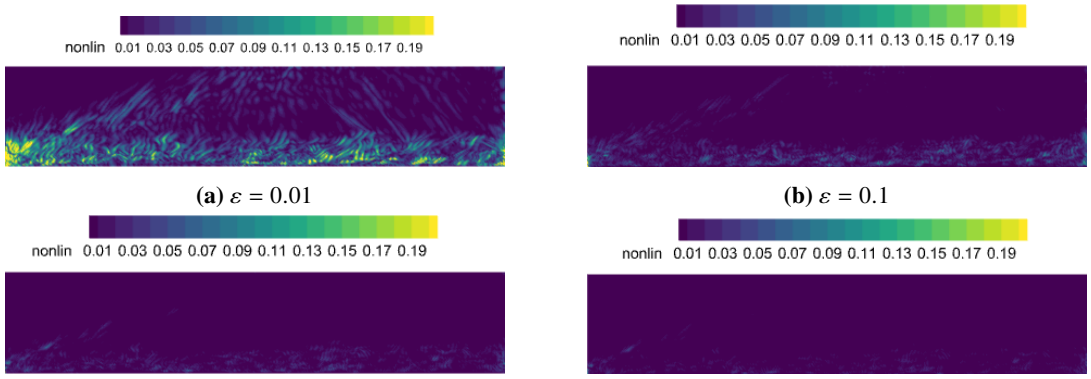

(a) $\varepsilon = 0.01$ **(b)** $\varepsilon = 0.1$

(c) $\varepsilon = 0.25$ **(d)** $\varepsilon = 0.5$

Fig. 5 Nonlinear shock sensor fields for the Mach 2.5 case. Equivalent to $1-$ flux, higher numbers mean more dissipation will be introduced at that location. Each graph has the same scale

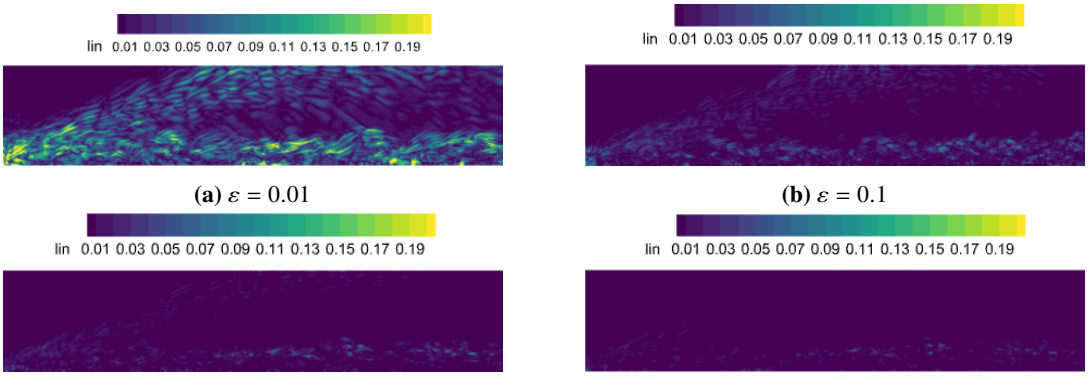

(a) $\varepsilon = 0.01$ **(b)** $\varepsilon = 0.1$

(c) $\varepsilon = 0.25$ **(d)** $\varepsilon = 0.5$

Fig. 6 Linear shock sensor fields for the Mach 2.5 case. Equivalent to $1-$ flux, higher numbers mean more dissipation will be introduced at that location. Each graph has the same scale

.

It can be seen that lower ε values lead to the introduction of more dissipation. As ε increases, the shock wave slowly fades, but the near wall turbulence still receives dissipation.

See Fig.7 for the time averaged flux limiter field. The smoothness of these plots in comparison to Fig.6, shows the importance of having a flux limiter that works at every timestep, and that it is not beneficial to simply mask an area and switch solvers there. Because of the unsteadiness of turbulence, it is important to integrate the limiter into the solver.

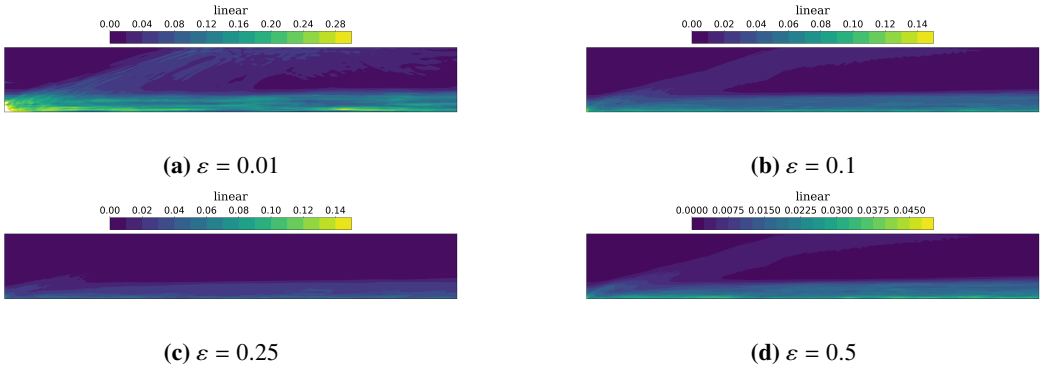

(a) $\varepsilon = 0.01$ **(b)** $\varepsilon = 0.1$

(c) $\varepsilon = 0.25$ **(d)** $\varepsilon = 0.5$

Fig. 7 Time average of linear shock sensor fields for the Mach 2.5 case.

.

C. Statistics

To benchmark the performance of each limiter, the Reynolds stresses are plotted and compared to the DNS data in Fig.8. In Fig.8.a it can be seen that the lower ε led to results that diverged more compared to a higher ε. This indicates that artificially introducing too much dissipation is harmful, and further shows the importance of optimizing the limiter so that the solution converges, but does so with accuracy. The shear stress graph in Fig.8.b shows that shear stresses are overestimated for each ε value, but each ε is overestimated the same amount. This indicates that the dissipation introduced for near wall turbulence artificially increased the shear stresses. Hence, having a sensor that is not sensitive to the broadband turbulence fluctuations, such as the Ducros sensor, would be more attractive than one that also attenuates physical turbulence gradients.

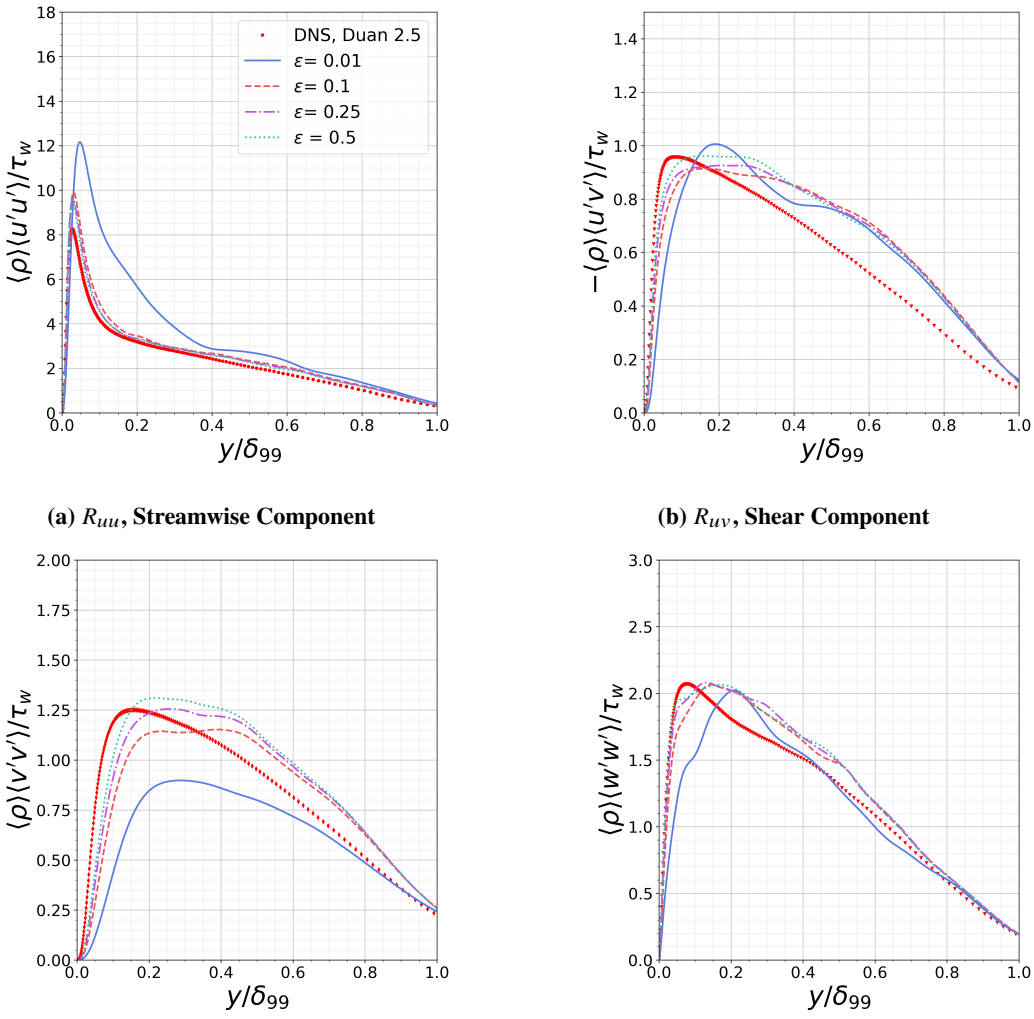

(a) R_{uu}, Streamwise Component

(b) R_{uv}, Shear Component

(c) R_{vv}, Wall-normal Component

(d) R_{ww}, Spanwise Component

Fig. 8 Reynolds stresses for the modified Van Leer case compared against the reference DNS. Red symbols correspond to the reference DNS case of Zhang et al. [23]. Black solid line corresponds to the baseline case.

The mean velocity is plotted in Fig.9. It is scaled using the same methods as in Fig.3. using Trettel-Larson[25].The higher the ε value, the closer the solution approaches the baseline case. In more sensitive schemes, the near wall velocity is artificially increased from the dissipation.

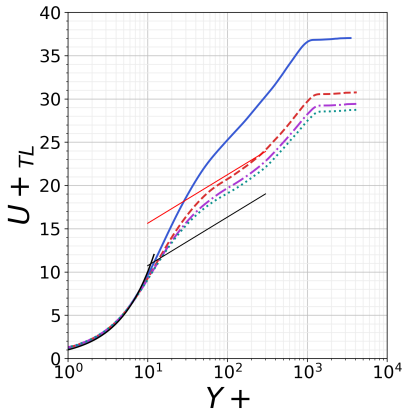

Fig. 9 Modified Van Leer case mean velocity profile compared against incompressible theory. Blue line represents $\varepsilon = 0.5$ and green dotted line represents $\varepsilon = 0.01$. Thin black line is the log-law given by Eqn. 10, with the thin red line corresponding to the same equation, except with y-intercept instead change to 10.

IV. Conclusion and Future Work

Further analysis of various limiting schemes should be conducted to find a balance between efficiency and accuracy. Further work will include analysis of the more complex Ducros flux limiter, as well as analysis of Mach 8 flow with a more defined shock. Another important case to consider is when there are shock boundary layer interactions, in order to ensure that an appropriate amount diffusion occurs in the correct places for convergence.

References

[1] Pirozzoli, S., "Conservative hybrid compact-Weno schemes for shock-turbulence interaction," *Journal of Computational Physics*, Vol. 178, No. 1, 2002, p. 81–117. https://doi.org/10.1006/jcph.2002.7021.

[2] Kravchenko, A. G., and Moin, P., "On the Effect of Numerical Errors in Large Eddy Simulations of Turbulent Flows," *Journal of Computational Physics*, Vol. 131, 1997, pp. 310–322.

[3] Ducros, F., Laporte, F., Soulères, T., Guinot, V., Moinat, P., and Caruelle, B., "High-order fluxes for conservative skew-symmetric-like schemes in structured meshes: Application to compressible flows," *Journal of Computational Physics*, Vol. 161, No. 1, 2000, p. 114–139. https://doi.org/10.1006/jcph.2000.6492.

[4] Smagorinsky, J., "General Circulation Experiments with the Primitive Equations. I. The Basic Experiment," *Monthly Weather Review*, Vol. 91, 1963, pp. 99–164.

[5] Speziale, C. G., "Galilean Invariance of Subgrid-Scale Stress Models in the Large Eddy Simulation of Turbulence," *Journal of Fluid Mechanics*, Vol. 156, 1985, pp. 55–62.

[6] Geurts, B. J., "Inverse Modeling for Large Eddy Simulation," *Physics of Fluids*, Vol. 9, No. 12, 1997, pp. 3585–3587.

[7] Stolz, S., and Adams, N. A., "An Approximate Deconvolution Procedure for Large Eddy Simulation," *Physics of Fluids*, Vol. 11, No. 7, 1999, pp. 1699–1701.

[8] Erlebacher, G., Hussaini, M. Y., Speziale, C. G., and Zang, T. A., "Toward the Large Eddy Simulation of Compressible Turbulent Flows," *Journal of Fluid Mechanics*, Vol. 238, 1992, pp. 155–185.

[9] Germano, M., Piomelli, U., Moin, P., and Cabot, W. H., "A Dynamic Subgrid-Scale Eddy Viscosity Model," *Physics of Fluids*, Vol. 3, No. 7, 1991, pp. 1760–1765.

[10] Moin, P., Squires, K., Cabot, W., and Lee, S., "A Dynamic Subgrid-Scale Model for Compressible Turbulence and Scalar Transport," *Physics of Fluids*, Vol. 3, No. 11, 1991, pp. 2746–2757.

[11] Lilly, D. K., "A Proposed Modification of the Germano Subgrid-Scale Closure Method," *Physics of Fluids*, Vol. 3, No. 11, 1992, pp. 633–635.

[12] Yoshizawa, A., "Statistical Theory for Compressible Turbulent Shear Flows, with the Application to Subgrid Modeling," *Physics of Fluids*, Vol. 29, No. 7, 1986, pp. 2152–2164.

[13] Eidson, T. M., "Numerical Simulation of the Turbulent Rayleigh-Bénard Problem Using Numerical Subgrid Modeling," *Journal of Fluid Mechanics*, Vol. 158, 1985, pp. 245–268.

[14] Jameson, A., "The Construction of Discretely Conservative Finite Volume Schemes that Also Globally Conserve Energy or Entropy," *Journal of Scientific Computing*, Vol. 34, 2008, pp. 152–187.

[15] Jameson, A., "Formulation of Kinetic Energy Preserving Conservative Schemes for Gas Dynamics and Direct Numerical Simulation of One-Dimensional Viscous Compressible Flow in a Shock Tube Using Entropy and Kinetic Energy Preserving Schemes," *Journal of Scientific Computing*, Vol. 34, 2008, pp. 188–208.

[16] Kuya, Y., Totani, K., and Kawai, S., "Kinetic Energy and Entropy Preserving Schemes for Compressible Flows by Split Convective Forms," *Journal of Computational Physics*, Vol. 375, 2018, pp. 823–853.

[17] Shima, N., Kuya, Y., Tamaki, Y., and Kawai, S., "Preventing Spurious Pressure Oscillations in Split Convective form Discretization for Compressible Flows," *Journal of Computational Physics*, Vol. 427, 2021, p. 110060.

[18] Kuya, Y., and Kawai, S., "High-Order Accurate Kinetic-Energy and Entropy Preserving (KEEP) Schemes On Curvilinear Grids," *Journal of Computational Physics*, Vol. 443, 2021, p. 110482.

[19] Oefelein, J. C., and Sankaran, R., "Large Eddy Simulation of Reacting Flow Physics and Combustion," *Exascale Scientific Applications: Programming Approaches for Scalability, Performance, and Portability*, edited by T. Straatsma, K. Antypas, and T. Williams, CRC Press, Taylor and Francis Group, Boca Raton, Florida, 2018, Chap. 11, pp. 231–256.

[20] Luo, L., Straatsma, T. P., Suarez, L. E. A., Broer, R., Bykov, D., D'Azevedo, E. F., Faraji, S. S., Gottiparthi, K. C., de Graaf, C., Harris, J. A., Havenith, R. W. A., Jense, H. J. A., Joubert, W., Kathir, R. K., Larkin, J., Li, Y.-W., Lyakh, D., Messer, O. E. B., Norman, M. R., Oefelein, J. C., Sankaran, R., Tillack, A. F., Barnes, A. L., Visscher, L., Wells, J. C., and Wibowo, M., "Pre-Exascale Accelerated Application Development: The Oak Ridge National Laboratory Summit Experience," *IBM Journal of Research and Development*, Vol. 64, No. 3/4, 2020, pp. 11:1–11:21.

[21] Schau, K. A., Purushotham, D., and Oefelein, J. C., "Programming Approaches for Scalability, Performance, and Portability of Combustion Physics Codes," *Proceedings of the Combustion Institute*, Vol. 39, 2023, pp. 5137–5144.

[22] van Leer, B., "Towards the ultimate conservative difference scheme. v. A second-order sequel to Godunov's method," *Journal of Computational Physics*, Vol. 32, No. 1, 1979, p. 101–136. https://doi.org/10.1016/0021-9991(79)90145-1.

[23] Zhang, C., Duan, L., and Choudhari, M. M., "Direct Numerical Simulation Database for Supersonic and Hypersonic Turbulent Boundary Layers," *AIAA Journal*, Vol. 56, No. 11, 2018, pp. 4297–4311.

[24] Schau, K. A., Johnson, C., Muller, J., and Oefelein, J. C., "An ensemble Synthetic Eddy Method for accurate treatment of inhomogeneous turbulence," *Computers & Fluids*, Vol. 248, 2022, p. 105671.

[25] Trettel, A., and Larsson, J., "Mean velocity scaling for compressible wall turbulence with heat transfer," *Physics of Fluids*, Vol. 28, No. 2, 2016. 026102.